RSC Advances

PAPER

View Article Online
View Journal | View Issue

Cite this: *RSC Adv.*, 2025, **15**, 48236

Synergistic catalysis of ionic liquid-modified ceria and silver-deposited activated carbon for the rapid and sensitive colorimetric detection of hydrogen peroxide

Muhammad Asad,[a] Mohibullah Shah,[b] Naeem Khan,[a] Anwar Iqbal,[c] Khaled Fahmi Fawy,[d] Xiaoping Zhang,[e] Wei Sun,*[e] Amir Badshah*[a] and Umar Nishan*[a]

Hydrogen peroxide (H_2O_2) is an important analyte that can indicate oxidative stress and cause DNA and protein damage. Natural peroxidases in the body have certain levels, and their abnormal concentrations can lead to the onset of oxidative stress and cancer. Hence, it is essential to monitor the level of H_2O_2 reliably and cost-effectively. The present study demonstrates the synthesis of silver and cerium oxide deposited on an activated carbon (Ag–CeO_2@AC) nanocomposite by applying a co-precipitation method. The nanocomposite was further functionalized with an ionic liquid (IL) to achieve better conductivity and deagglomeration. Various analytical techniques, such as XRD, EDS, XPS, FTIR spectroscopy, elemental mapping, HRTEM, and scanning electron microscopy (SEM), were used to confirm the synthesis of the nanocomposite. For the non-enzymatic colorimetric detection of H_2O_2, the IL-Ag-CeO_2@AC nanocomposite was employed as a peroxidase-like catalyst. Results showed the peroxidase-like activity of IL-Ag-CeO_2@AC in the presence of H_2O_2 and the chromogenic substrate tetramethylbenzidine (TMB). TMB was oxidized to oxTMB (blue-green color) with the maximum absorption at 652 nm in the presence of the analyte (H_2O_2). The catalytic activity of the proposed sensor was enhanced by optimizing various parameters, namely, the amount of the synthesized nanocomposite, time, pH, and TMB concentration. Once the experimental conditions were determined, the key analytical parameters of the proposed sensor were calculated. The linear range was found to be 10–190 μM, with limits of quantification and detection (LOQ and LOD) of 0.77 μM and 0.232 μM, respectively, and a regression coefficient (R^2) value of 0.996. In addition to its exceptional sensitivity, the sensor showed excellent selectivity for the detection of H_2O_2 under the influence of different possible interferents. The developed approach was utilized to determine H_2O_2 in real samples and demonstrated good feasibility and reproducibility.

Received 28th August 2025
Accepted 16th November 2025

DOI: 10.1039/d5ra06434a

rsc.li/rsc-advances

1. Introduction

Hydrogen peroxide (H_2O_2) is a byproduct of various biochemical reactions in the human body. Its concentration is controlled by the natural peroxidases present in the body. It is involved in various functions such as cell signaling, vascular remodeling, and activation of the immune system. However, its higher-than-normal concentration can indicate pathological conditions, such as oxidative stress and increased vulnerability to different types of cancers. Its increased concentration contributes to the damage of DNA and proteins, and hence, it is a contributing factor in cancer initiation and progression. In addition, it is present at several-fold higher concentrations in cancer cells than in normal cells. Thus, it can also be used as a means of monitoring the effects of chemotherapy or other forms of cancer treatments.[1] Therefore, it is of immense importance to develop sensors that can easily, efficiently, and cost-effectively monitor the levels of this important biomarker in a user-friendly manner.

For monitoring H_2O_2, various approaches have been reported, including chromatographic,[2] electrochemical,[3] chemiluminescence,[4] spectrophotometry,[5] and fluorescence

[a]*Department of Chemistry, Kohat University of Science and Technology, Kohat 26000, KP, Pakistan. E-mail: amirqau@yahoo.com; umarnishan85@gmail.com*
[b]*Department of Biochemistry, Bahauddin Zakariya University, Multan 66000, Pakistan*
[c]*Department of Chemical Sciences, University of Lakki Marwat, KP, Pakistan. E-mail: sunwei@hainnu.edu.cn*
[d]*Department of Chemistry, Faculty of Science, Research Center for Advanced Materials Science (RCAMS), King Khalid University, P.O. Box 960, Abha, 61421, Saudi Arabia*
[e]*Hainan International Joint Research Center of Marine Advanced Photoelectric Functional Materials, College of Chemistry and Chemical Engineering, Hainan Normal University, Haikou 571158, P. R. China*

techniques.[6] Although these techniques offer different merits, they also suffer from various shortcomings. They require highly skilled operators; in terms of instrumentation, they are expensive to acquire and sustain. In addition, they are generally not suitable for on-site analysis, are time-consuming in most cases, and require complex sample pretreatment steps. To circumvent the mentioned and other challenges associated with these techniques, colorimetric sensors provide a viable alternative. It is easy to use, rapid, sensitive, and selective, and the progress of its reaction can be monitored with the naked eye.[7,8]

Conventionally, colorimetric sensors are fabricated based on natural enzymes. Among natural enzymes, horseradish peroxidase and alkaline phosphatase have led the pack in the fabrication of colorimetric sensors. However, the intrinsic limitations of natural enzymes, such as cost and sensitivity to changes in temperature, pH, and other environmental factors, compromise their viability. These shortcomings have led to a significant reduction in the fabrication and application of colorimetric sensors. However, the rise of nanozymes has proven to be a much-needed impetus for the development of colorimetric-based sensor technologies.[9] The rise of nanotechnology has increased access to nanomaterials, which has led to the development of new colorimetric nanosensors. However, colorimetric nanosensors in their infancy are mainly based on expensive noble metal nanoparticles, such as platinum, palladium, and gold. Although the use of these metal-based nanosensors has proven effective, they suffer from elevated costs associated with these metals. This has led to the need for alternative approaches based on low-cost nanomaterials that deliver nanosensors with the desired sensitivity and selectivity without burdening the end user financially.

In this regard, metal oxide nanocomposites[10] and carbon-based, metallic,[11] and metal oxides[12] have been reported. However, there is a need for further platforms that can deliver the required results cost-effectively. Various oxides such as vanadium pentoxide, cobalt oxide, copper oxide, and iron oxide have been used as peroxidase mimics. Among the various metal oxides, nanoceria has been extensively applied in the fields of electrochemistry, gas sensors, photochemistry, catalysis, and luminescence.[13] Ceria has shown the intrinsic ability of mimicking the activity of several redox enzymes due to the existence of cerium in different oxidation states. However, owing to its semiconductor nature and the high bandgap value of 3.4 eV,[14] the properties of ceria can be enhanced by the addition of different kinds of impurities. Among them, silver is an excellent candidate because its interaction with ceria increases the exchange of absorbed oxygen with lattice oxygen. This results in structural defects at the interface of silver and ceria and weakens the cerium and oxygen linkage.[15] However, nanomaterials have various shortcomings that hinder their use. They have a high surface energy, resulting in the agglomeration and loss of the surface area necessary for their catalytic role. This has made it necessary to employ various types of matrix materials that retain the surface area of nanomaterials. Certain properties, like biocompatibility, easy availability, cost-effectiveness, electron mobility, and environmental friendliness, are considered prerequisites for the selection of any material as a possible matrix material.

Among them, activated carbon is a promising candidate owing to its biocompatibility, porosity, large surface area, high electrical conductivity, ubiquitous precursors, and availability. Activated carbon has been used for metal extraction, environmental applications, energy storage, catalysis, water treatment, and gas and air purification. It can effectively absorb a wide range of chemicals and bacterial nutrients.[7] To further enhance the conductivity of the system and impart its unique properties based on the synergy of various materials, ionic liquids (IL) have been used. ILs are currently gaining importance as potential stabilizers due to their useful chemical and physical characteristics, including low surface tension, high ionic conductivity, very low volatility, and effective dispersion. In particular, an IL consisting of 1-H-3-methyl imidazolium acetate was used.

This research demonstrates a unique combination of IL-Ag-CeO_2@AC nanocomposite aimed at the colorimetric sensing of hydrogen peroxide with outstanding sensitivity and selectivity. The synergistic effect of various constituents of the nanocomposite catalyzes the peroxidase-mimicking behavior of the fabricated nanozyme. The proposed sensor is being reported under its optimal conditions following comprehensive optimization. The effect of the matrix was also studied, and various potential interferents were tested in which hydrogen peroxide stood out. Finally, the optimized sensor was successfully used to estimate hydrogen peroxide in real matrices, showing reliable results.

2. Methodology

2.1 Chemicals

This study utilized various chemicals, namely cerium nitrate hexahydrate (99%), 3,3′,5,5′-tetramethylbenzidine, dimethyl sulfoxide, hydrochloric acid (37%), silver nitrate (99%), sodium hydroxide (97%), and hydrogen peroxide (35%), procured from Sigma-Aldrich, USA, and employed as received without further purification. Deionized water produced in the lab was used throughout the whole experiment. Blood serum samples were collected from Al-Habib Lab, Kohat (Khyber Pakhtunkhwa, Pakistan).

2.2 Instrumentation

UV-vis absorption spectra were recorded using a double-beam PerkinElmer spectrophotometer (Shimadzu UV 1800, Japan). To unveil the functional groups present in the synthesized material, Fourier-transform infrared (FTIR) spectroscopy was performed using a Thermo Nicolet Waltham, MA 5700 spectrometer. The range selected was 4000–400 cm^{-1}. The elemental composition and morphology of the prepared material were examined using ZEISS Gemini 500 from Germany. Using high-resolution transmission electron microscopy (HRTEM) with a JEM-2100F microscope (JEOL, Japan), high-resolution images were taken. To study the crystalline phase of the nanocomposite, a Bruker AXS D8 X-ray diffractometer operating with Cu Kα radiation was employed. To study the chemical state and

composition, X-ray photoelectron spectroscopy (XPS), Thermo, USA, was employed to examine the obtained material.

2.3 Synthesis of the nanocomposite

The desired nanocomposite (Ag–CeO_2@AC) was synthesized using a simple co-precipitation method with $Ce(NO_3)_3 \cdot 6H_2O$ and $AgNO_3$ on the surface of activated carbon. Briefly, a 0.03 M aqueous solution of cerium nitrate hexahydrate was mixed with a 0.4 M aqueous solution of silver nitrate. Subsequently, 6 g of activated carbon was mixed with the salt solution and stirred thoroughly. Overall, the ratio of the activated carbon and metal salts was kept at 9 : 1. After that, 0.03 M KOH solution was added to the mixture until its pH reached 11. The solution was kept on a magnetic stirrer for 4 hours at 2000 rpm. Finally, the precipitated product was obtained and washed several times with methanol and distilled water. The obtained precipitate was dried in an oven and calcined under an inert atmosphere at 300 °C for 3 hours. The synthesized nanocomposite was further functionalized with ionic liquid to obtain IL-Ag-CeO_2@AC using an earlier reported methodology with slight modifications.[8]

2.4 Procedure for sensing hydrogen peroxide

For the colorimetric detection of hydrogen peroxide, various combinations of the fabricated enzyme mimic (IL-Ag-CeO_2@AC), TMB, pH, and the analyte were tested under different time intervals. Three related but different experiments were carried out to ascertain the catalytic role of the synthesized nanozyme. For this purpose, initially, the TMB and the nanozyme were mixed together, and the response was noted. After that, a combination of TMB and hydrogen peroxide was also tested. Finally, in another experiment, a combination of TMB, nanozyme, and hydrogen peroxide was tested. All the reactions were visually observed, captured through a smartphone, and confirmed through UV-visible spectrophotometry. To obtain the maximum out of the fabricated sensor, various experimental parameters affecting its performance were optimized. For this purpose, the standard approach used in analytical chemistry was used. Briefly, one variable varied, while the others were kept constant. The amount of mimic enzyme, TMB concentration, pH, and time were optimized one after the other. The optimized sensor was applied to the blood serum samples of the diabetic patients. The blood samples underwent centrifugation at 4000 rpm for 15 minutes. Furthermore, under the same experimental conditions, hydrogen peroxide was detected in the real samples using the spiking approach. Approval for the research was obtained from the Kohat University of Science and Technology Ethical Committee (Ref: KUST/Ethical Committee/1628). Informed consent was obtained for any experimentation with the human subjects.

3. Results and discussion

3.1 Characterization

3.1.1 FTIR analysis of the prepared nanocomposite. Fig. 1(i) shows the FTIR spectrum of the synthesized Ag–CeO_2@AC nanocomposite in the range of 4000–400 cm^{-1}. The peaks observed at 482 and 610 cm^{-1} can be attributed to spectral metal–oxygen bonding. The peak found at 1110 cm^{-1} indicates the presence of an ether linkage.[16] The peak observed at 1616 cm^{-1} indicates the presence of sp^2 carbon in the synthesized material. The band at 2350 cm^{-1} indicates the stretching vibration of the adsorbed carbon dioxide. The broad peak around 3436 cm^{-1} is due to the stretching vibration of the hydroxyl group coming from the adsorbed water.

3.1.2 XRD spectrum of the prepared nanocomposite. The crystalline nature of the synthesized Ag–CeO_2@AC nanocomposite was ascertained using the X-ray diffraction technique, as shown in Fig. 1(ii). The major peaks of ceria in the synthesized nanocomposite are shown at 2θ values of 28.5°, 33.2°, 50.2°, 56.4°, 59.2°, 69.4°, and 76.8° with crystalline planes (111), (200), (220), (311), (222), (400), and (331), respectively (JCPDS 34-0394). Similarly, the peaks observed at 2θ values of 38.31°, 44.47°, and 63.82° with space planes of (111), (200), and

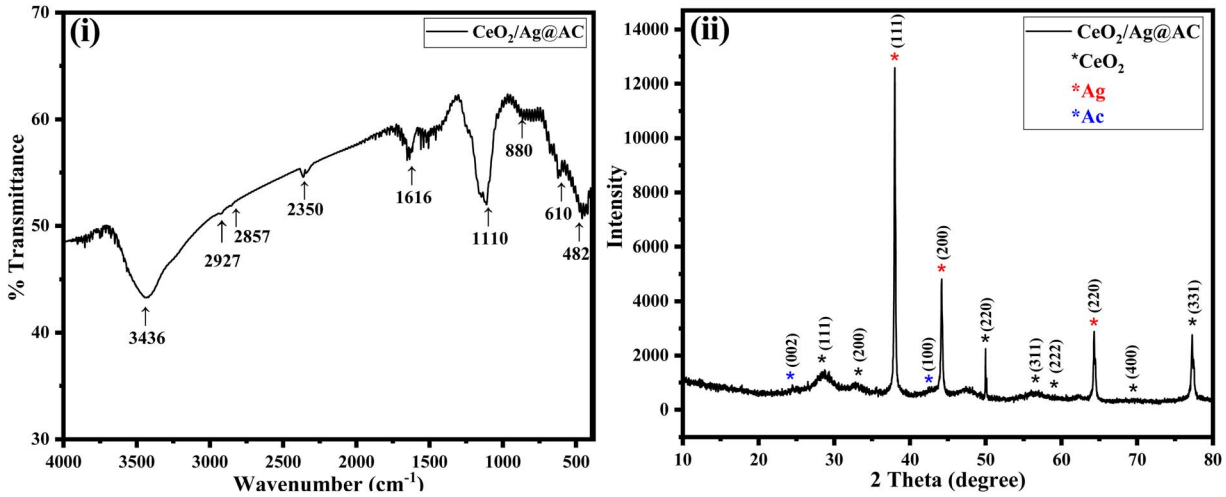

Fig. 1 (i) FTIR spectrum of the Ag–CeO_2@AC nanocomposite with the characteristic metal oxide bonding in the fingerprint region. (ii) X-ray diffraction analysis showing the corresponding peaks of the constituents of the synthesized Ag–CeO_2@AC nanocomposite.

(220), respectively, correspond to silver (JCPDS 04-0783). In addition, the two peaks observed in the Ag–CeO_2@AC at 2θ values of 23.21° and 43.55° with crystalline planes of (002) and (100) correspond to the activated carbon.[17] The average crystallite size of the prepared nanocomposite was calculated using the Scherrer equation, which was found to be 45.60 nm.

3.1.3 Morphological study of the nanocomposite. A detailed morphological study was performed to observe the surface characteristics of the nanocomposite, as shown in Fig. 2. From SEM image 2A, an irregular shape can be observed for the nanocomposite. The elemental analysis through EDS showed the presence of C, O, Ag, and Ce, with the corresponding weight and atomic percentage given for each element in the inset table, as shown in 2B. Fig. 2C and D present the TEM and HRTEM images of the synthesized nanocomposite, respectively. TEM image 2C shows the deposition of the metal nanoparticles over the surface of the activated carbon, which functions as a matrix material. The HRTEM image 2D shows the lattice fringes of the metals deposited and distributed over the matrix surface. Fig. 2(E–I) shows the elemental mapping results of the synthesized nanocomposite. Image 2E shows the overlay consisting of all the elements detected in the fabricated nanocomposite. Subsequent images demonstrate the uniform distribution of carbon, oxygen, silver, and cerium elements on the synthesized nanocomposite.

3.1.4 X-ray photoelectron spectroscopy (XPS) spectra of the CeO_2/Ag@AC nanocomposite. Using the XPS technique, the valence state of the surface atoms in the fabricated Ag–CeO_2@AC nanocomposite was analyzed. Fig. 3A demonstrates the survey spectrum of the prepared nanocomposite. It shows dominant peaks for C, Ag, O, and Ce. The survey spectrum peaks were deconvoluted to gain further insight into the elements present in the fabricated nanocomposite. Fig. 3B illustrates the deconvoluted spectrum of ceria with binding energy values of 882.4 eV, 889.1 eV, 897.8 eV, 901.3 eV, 907.5 eV, and 916.3 eV, indicating the presence of the Ce 3d form of cerium. The peaks of Ce 3d contain doublet spin orbits, such as Ce $3d_{3/2}$ (882.4 eV) and Ce $3d_{5/2}$ (916.3). Furthermore, the binding energies correspond to the main oxidation states of Ce 3d, such as Ce^{3+} and Ce^{4+}. In addition, the results show some satellite peaks corresponding to μ1, μ2, ν1, and ν2 with Ce $3d_{3/2}$ and Ce $3d_{5/2}$ peaks.[18] Fig. 2C demonstrates the deconvoluted spectrum of O 1s, which shows two major peaks at 529.3 eV and 532.4 eV. They are assigned to adsorbed oxygen ions and lattice oxygen ions.[19] Fig. 3D shows the high-resolution XPS spectrum of C 1s. In the spectrum, the peaks observed at binding energy values of 284.8 eV, 285.3 eV, and 288.4 eV are assigned to (C–O) and (C=O), indicating that organic carbon is present in the prepared nanocomposite. However, the high-resolution XPS spectra of Ag 3d show metallic Ag peaks at a binding energy of

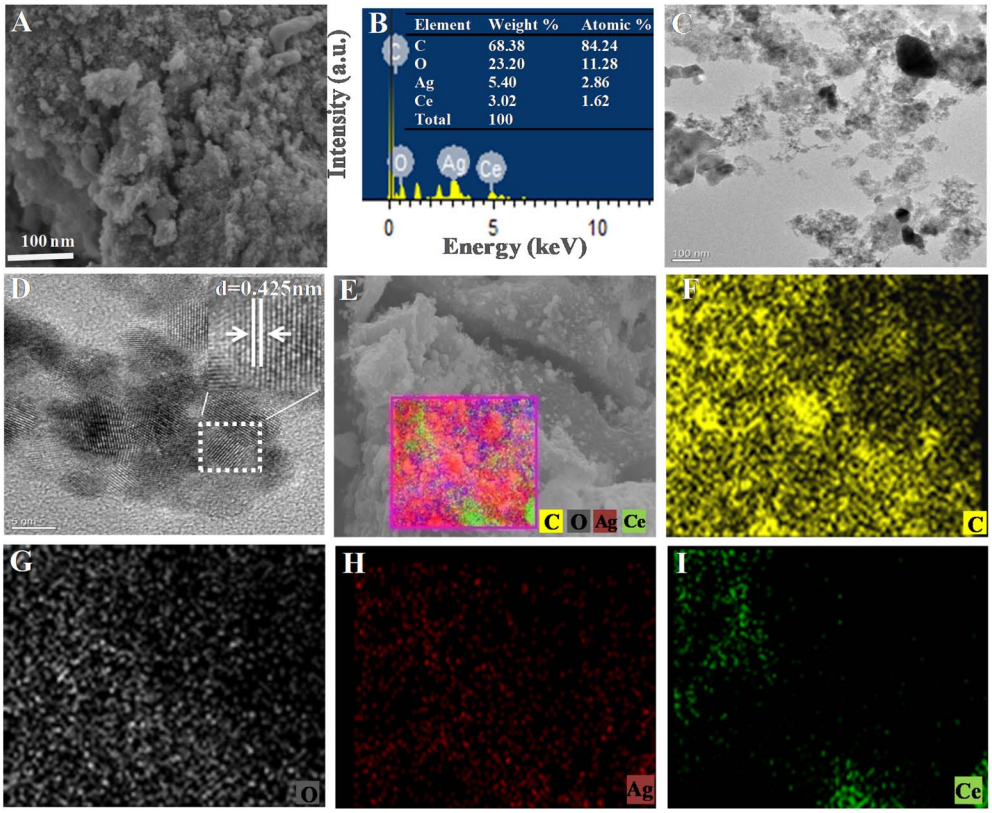

Fig. 2 (A) SEM image with irregular surface morphology of the synthesized nanocomposite. (B) EDS spectrum of the synthesized material with the atomic and weight percentages of the elements present in the nanocomposite. (C and D) TEM and HRTEM images demonstrating the distribution of the nanoparticles on the matrix and lattice fringes of the deposited metals, respectively. (E–I) Elemental distribution in the synthesized nanocomposite. The uniform distribution of the elements shows the desired synthesis.

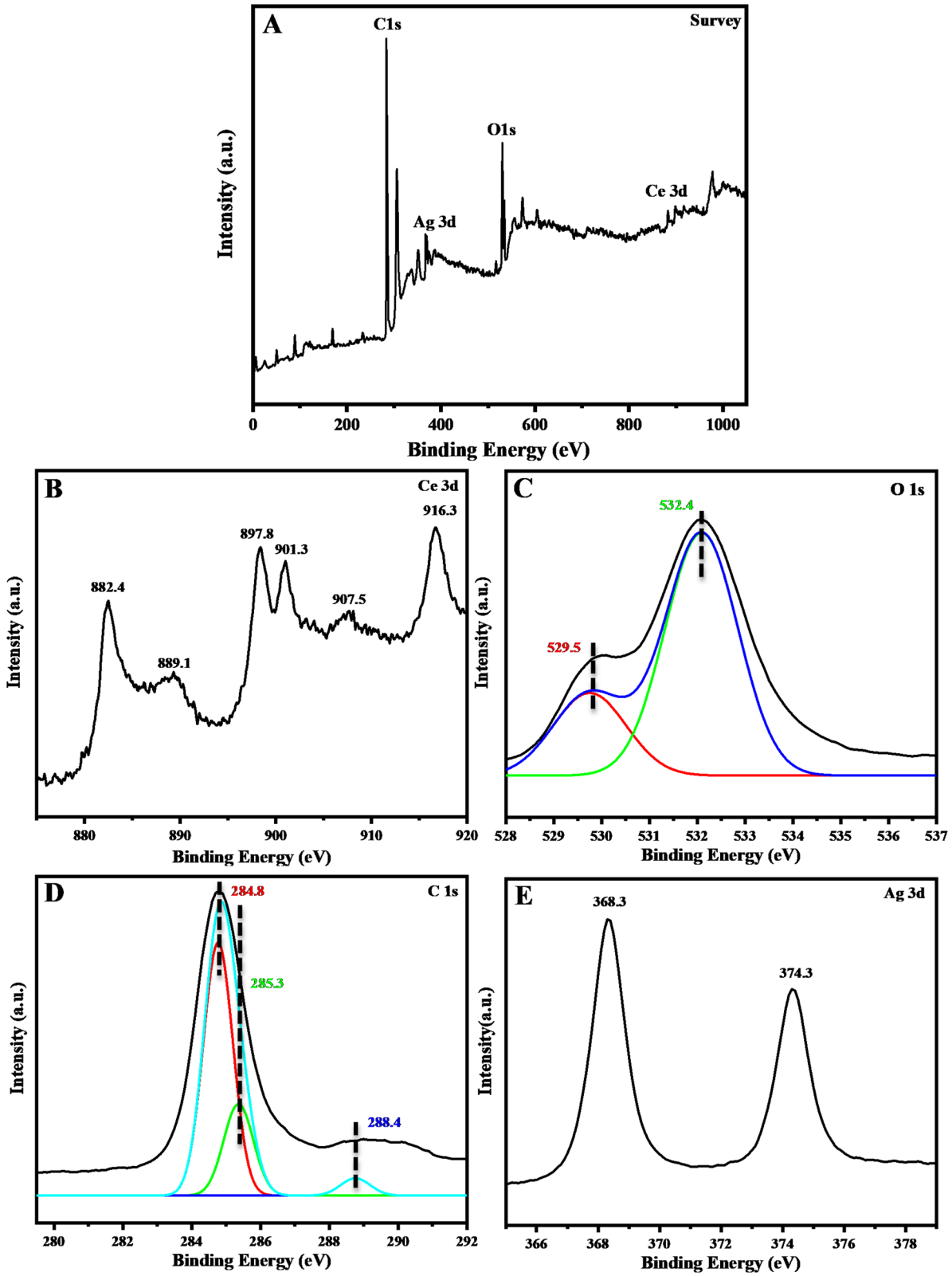

Fig. 3 XPS analysis of the prepared Ag–CeO_2@AC nanocomposite showing the surface oxidation states of the constituent elements. (A) Survey spectrum confirming the existence of C, Ag, O, and Ce. (B) Deconvolution analysis of the spectrum for cerium, indicating the presence of Ce 3d, Ce $3d_{3/2}$, and Ce $3d_{5/2}$ with satellite peaks. (C) Deconvoluted spectrum of O 1s showing two major peaks at 529.3 eV and 532.4 eV, corresponding to adsorbed oxygen and lattice oxygen ions. (D) Peaks assigned to C–O and C=O linkages. (E) Binding energies of 374.3 eV and 368.3 eV assigned to Ag $3d_{3/2}$ and Ag $3d_{5/2}$, respectively.

374.3 eV (Ag $3d_{3/2}$) corresponding to Ag^{+} and 368.3 eV (Ag $3d_{5/2}$) corresponding to Ag^{0} with a spin energy separation of 6 eV, as shown in Fig. 3E.[20]

3.2 Colorimetric sensing of hydrogen peroxide

As mentioned in the methodology section, three experiments were performed. In the first experiment represented by curve *A*, the synthesized nanocomposite and TMB were taken together. No visible colorimetric change could be observed. The spectrophotometry reading also confirmed this observation, indicating no peak. In another experiment, hydrogen peroxide and TMB were taken together, which were represented by Eppendorf tube B and curve *B*. A minimal colorimetric change with a very light blue-green color was observed. The spectrophotometric reading confirmed a small peak in the oxidized form of the TMB. Finally, when the proposed mimic enzyme (IL-Ag-CeO_2@AC), TMB, and hydrogen peroxide were taken together, which was represented by curve *C*, a clear blue-green color of the oxidized form of TMB was visible to the naked eye. The spectrophotometric reading confirmed a peak of TMB at 652 nm. This confirmed the peroxidase-mimetic behavior of the developed nanozyme IL-Ag-CeO_2@AC. During the course of these reactions, the amounts of various constituents of the sensing system were taken to be 55 μL of the mimic enzyme, 110 μL of 22 mM TMB, 130 μL of PBS solution (pH 5), and 100 μL of 200 μM H_2O_2 solution Fig. 4.

3.3 Proposed mechanism

The enhancement in catalytic activity arises due to the synergistic interaction between ceria and silver nanoparticles present in the nanocomposite. In this case, ceria provides redox-active Ce^{3+}/Ce^{4+} sites that promote the generation of reactive oxygen species. At the same time, silver nanoparticles act as electron mediators and transfer electrons for the decomposition of hydrogen peroxide. At the same time, the combination of both also produces charge separation, which leads to high performance compared to individual nanoparticles. The peroxidase-like activity of the prepared enzyme mimic (IL-Ag-CeO_2@AC) is not present in the case where no hydrogen peroxide was used. In the absence of the hydrogen peroxide, no substrate is present for the peroxidase-like action of the synthesized mimic enzyme. However, in the absence of the mimic enzyme, the combination of hydrogen peroxide and TMB produces a minimal change. A light blue-green color of oxTMB appears with a small peak at 652 nm, showing the oxidation of TMB to a very small extent. This can be attributed to the fact that a minimal amount of hydroxyl free radicals is generated in the absence of the mimic enzyme. However, the combinations of the proposed mimic enzyme, hydrogen peroxide, and TMB result in the transformation of the transparent mixture into an intense blue-green color characteristic of oxTMB. This colorimetric change is attributed to the mimic enzyme (IL-Ag-CeO_2@AC), which, by virtue of its peroxidase-like activity, helps in the generation of a large number of hydroxyl free radicals. The generation of these radicals expedites the oxidation of TMB, resulting in the formation of oxTMB with the appearance of its characteristic color (blue-green with a peak at 652 nm). Chemically, this change in color can be explained by the conversion of the benzoid form of TMB (transparent) into the quinoid (blue-green) form. As a result of this transformation, conjugation increases; hence, the energy gap between the frontier orbitals decreases. The decrease in the energy gap of frontier orbitals results in absorption in the visible region, which was previously possible only in the UV region.[21] Using the chemical scavenger method with thiourea and t-butanol, the generation of hydroxyl

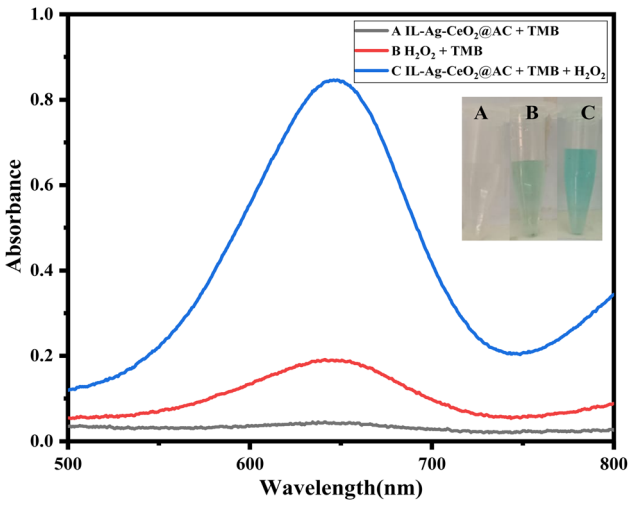

Fig. 4 Confirmation of the peroxidase-like action of the synthesized mimic enzyme. Curve *A* (inset Eppendorf tube A) demonstrates that only the mimic enzyme and TMB show no reactivity, as represented by a straight line. Similarly, curve *B* (inset Eppendorf tube B) demonstrates that the combination of TMB and hydrogen peroxide gives a minimal amount of the oxidized form of TMB. The combination of the mimic enzyme, TMB, and hydrogen peroxide, represented by curve *C*, (inset Eppendorf tube C) shows an intense peak for oxTMB, confirming the peroxidase-mimicking catalytic activity of the prepared nanozyme.

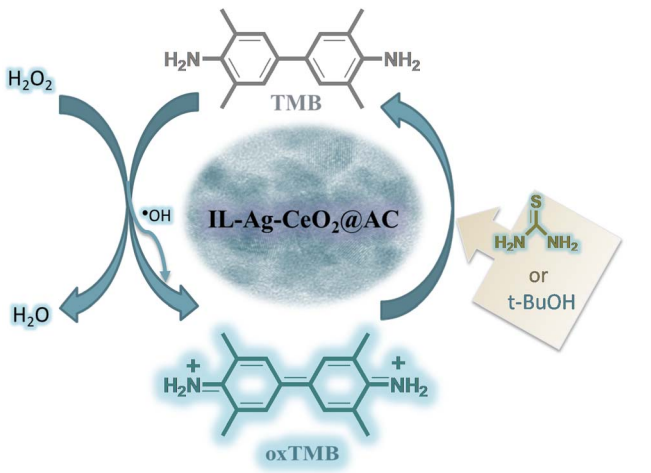

Scheme 1 Schematic of the sensing mechanism of hydrogen peroxide by the catalytic activity of the IL-Ag-CeO_2@AC mimic enzyme in the presence of TMB. The catalytic inhibition is achieved through the use of thiourea and t-butanol.

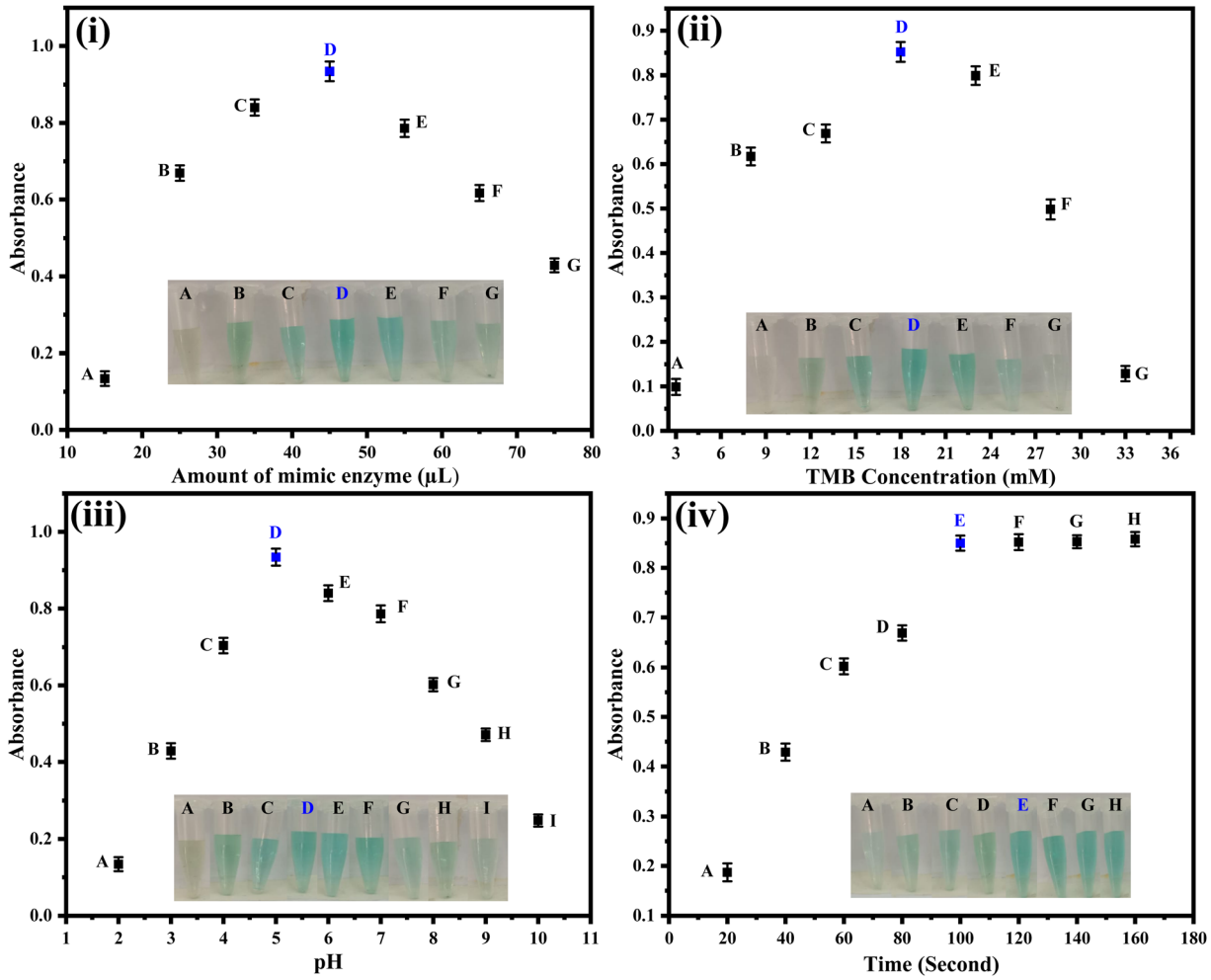

Fig. 5 (i) Effect of the amount of mimic enzyme, with the optimal response attained at 45 µL as shown by the inset Eppendorf tubes A–G. (ii) Optimization of TMB concentration with the maximum activity at 18 mM as shown by the inset Eppendorf tubes A–G. (iii) Effect of pH on the proposed sensor, with the excellent catalytic activity observed at pH 5.5 as shown by the inset Eppendorf tubes A–I. (iv) Effect of time in the range of 20–160 seconds as shown by the inset Eppendorf tubes A–H. The maximum absorbance was observed at 100 seconds and used for the subsequent experiments.

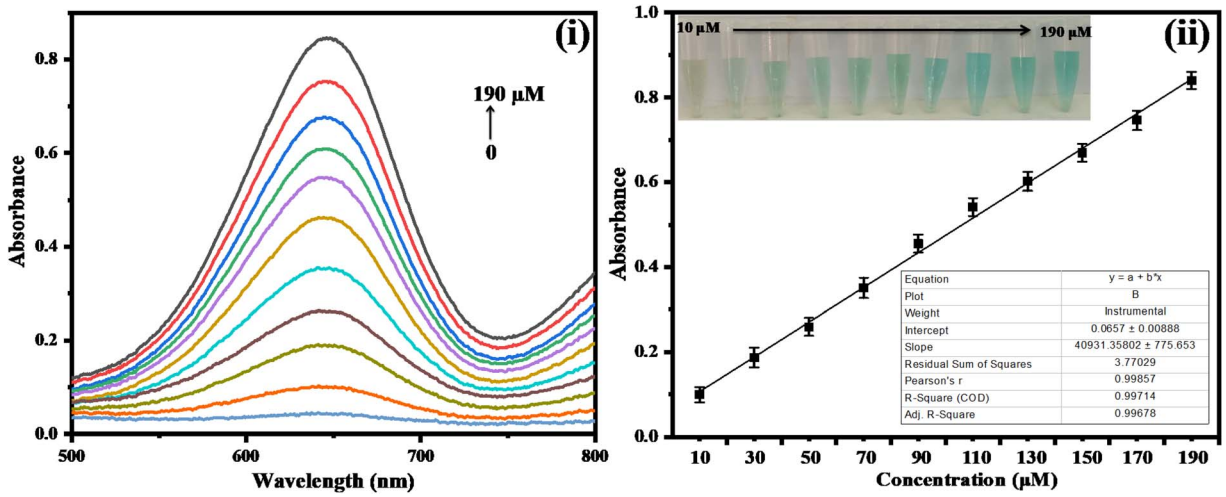

Fig. 6 (i) UV-vis absorption spectra of various concentrations of H_2O_2 ranging from 10 to 190 µM. (ii) Linear calibration plot and the color change (inset) in the developed assay at various concentrations (10–190 µM) of H_2O_2, with an R^2 value of 0.996.

Table 1 Comparison of the LOD and linear range of the developed assay using different nanomaterial-based colorimetric methods for H_2O_2 determination

S. NO	Material used	Method applied	LOD (μM)	Linear range (μM)	References
1	Ag@TPE-SiO_2 NPs	Colorimetric	2.1	5–160	22
2	Cu(II)-coated Fe_3O_4 NPs	Colorimetric	0.2	2.5–100	23
3	IL-cappedAg-Fe_2O_3	Colorimetric	0.086	0.001–0.36	21
3	h-Fe_3O_4@ppy	Colorimetric	0.18	0.2–100	24
4	Ag–CoO NPs	Colorimetric	3.47	1–100	25
5	ZnTPyP-DTAB NPs	Colorimetric	0.5	8–50	26
6	Fe_3O_4 NPs/MIL-53(Al)	Colorimetric	0.8499	1–20	27
7	$CuWO_4$ NPs	Colorimetric	0.2	24.87–3600	28
8	NiNPs-IL	Colorimetric	120	400–4000	29
9	IL-Ag-CeO_2@AC	Colorimetric	0.23	10–190	Present work

free radicals was confirmed indirectly. The addition of these scavengers resulted in no change in the color of TMB even in the presence of the mimic enzyme and hydrogen peroxide. This confirmed that the change in color of the chromogenic substrate can be attributed to the generation of hydroxyl free radicals, which are catalyzed by the mimic enzyme. The schematic representation of the proposed reaction is illustrated in Scheme 1.

3.4 Optimization of various experimental parameters

A number of factors affect the performance of a colorimetric sensor. They were optimized in order to report on the optimal performing parameters for the proposed sensor. Fig. 5(i) shows the effect of the amount of the mimic enzyme in the range of 15–75 μL. The optimal catalytic activity of the proposed sensor was observed at 45 μL and hence used for onward reactions. Fig. 5(ii) demonstrates the optimization of the TMB concentration in the range of 3–33 mM, and the best response was achieved at 18 mM. The optimal amount of TMB ascertained was used for the onward experiments. The effect of pH on the performance of the proposed sensor was studied in the range of 2–10, as shown in Fig. 5(iii). The optimal response was observed at pH 5.5 and used for subsequent reactions. Fig. 5(iv) shows the effect of time on the performance of the proposed sensor in the range of 20–160 seconds. The best response was achieved in 100 seconds and was thus used in the subsequent experimental procedure.

3.5 Analytical assessment of the developed sensor

After comprehensive optimization and reporting on the optimal conditions for the fabricated sensor, it was tested for its linearity, precision, accuracy, and sensitivity. Different concentrations of hydrogen peroxide were tested, and the absorbance spectra of the solution were recorded, as shown in Fig. 6(i). The results showed a quantitative linearity in absorbance with the increase in the concentration of hydrogen peroxide in the range of 10–190 μM. From the absorbance spectra, a calibration graph was plotted, as shown in Fig. 6(ii). Although hydrogen peroxide could be detected qualitatively beyond the mentioned linear range of 10–190 μM, the quantitative relationship could not be ascertained. Other parameters, such as R^2 (regression coefficient), were calculated to be 0.996. Based on the equations LOD $= 3.3\sigma/s$ and LOQ $= 10\sigma/s$, where s represents the slope of the curve and σ shows the SD of ten blank samples, the limit of detection and limit of quantification of the developed sensor were found to be 0.232 μM and 0.77 μM, respectively. Table 1 presents a comparison of the LOD and linear range of the developed sensor with previously reported nanomaterial-based colorimetric sensors. The proposed sensor showed excellent performance in terms of linear range, LOD, and LOQ.

3.6 Selectivity study

The key parameter of selectivity of the proposed assay was studied in the presence of various species that could show interference. For this purpose, equimolar concentrations of the interferents and hydrogen peroxide were taken under the prevailing reported optimized conditions. Various species, such as uric acid, ascorbic acid, urea, citric acid, dopamine, lead, and nitrite, were tested alongside hydrogen peroxide. The results indicate that complete oxidation of

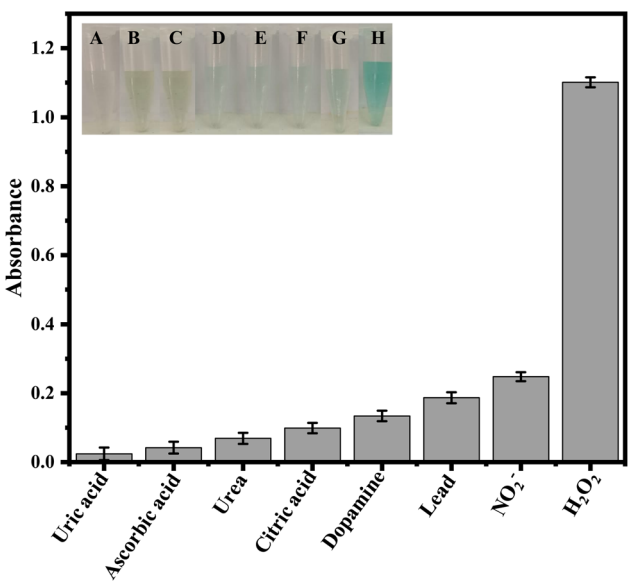

Fig. 7 Interference study of the proposed assay for the determination of H_2O_2 in the presence of potential interfering species, such as urea, ascorbic acid, uric acid, fructose, glucose, lactose, and maltose, at a concentration of 190 μM.

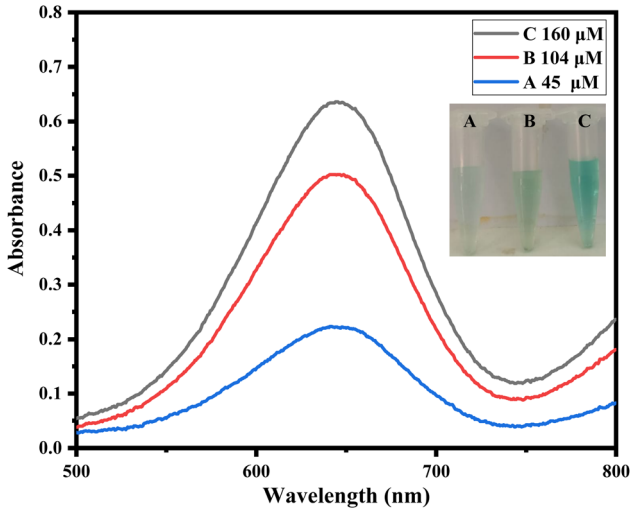

Fig. 8 Determination of H_2O_2 in real samples in the linear range of the developed sensor alongside the inset Eppendorf tubes.

Table 2 Detection of H_2O_2 in blood serum samples

Samples	Detected (μM)	H_2O_2 added (μM)	H_2O_2 found (μM)	Recovery (%)	RSD (%)
1	3	42	45	107.14	0.431
2	4	100	104	104	0.502
3	7	153	160	103.89	0.732

TMB was only possible in the presence of hydrogen peroxide. The presence of other species did not show any significant colorimetric change. The reactions were observed with the naked eye, and confirmation was achieved using a spectrophotometric approach, as shown in Fig. 7.

3.7 Real sample application of the developed sensor

To investigate the practical application of the developed sensor, H_2O_2 was detected in blood serum samples. For this purpose, blood serum samples were collected from diabetic patients and processed for further use. Using the standard addition method, known concentrations of H_2O_2, such as 42, 100, and 153 μM, were spiked into the real samples.[30] The concentration of H_2O_2 in the real samples was calculated from an already developed calibration plot. The results of the proposed assay are summarized in Fig. 8 and Table 2. The obtained results clearly indicate that the developed sensor can be used for the detection of hydrogen peroxide in real samples.

4. Conclusions

This study presented the synthesis and confirmation of the Ag–CeO_2@AC nanocomposite. Advanced physico-chemical techniques, such as FTIR spectroscopy, XRD, SEM, HRTEM, EDS, XPS, and elemental mapping, confirmed the desired synthesis, corroborating each other's findings. The synthesized nanocomposite was functionalized using an ionic liquid to benefit from the synergy and obtain IL-Ag-CeO_2@AC. The obtained nanocomposite demonstrated remarkable peroxidase-like activity and produced a blue-green color characteristic of oxTMB. Optimization experiments were performed to fine-tune the performance of the fabricated sensor. The developed platform demonstrated an impressive linear range of 10–190 μM with an LOQ of 0.77 μM, an LOD of 0.232 μM, and an R^2 value of 0.996. The reported platform, alongside its excellent sensitivity, was also selective in the presence of various other potential interfering species under the optimum experimental conditions. The developed sensor was also applied to detect H_2O_2 in real blood serum samples within the linear range of the fabricated platform. The proposed sensor has all the potential to be used as a laboratory tool to monitor hydrogen peroxide in a diverse range of samples, thereby benefiting the healthcare community, industry, and the general public.

Conflicts of interest

The authors declare no conflict of interest.

Data availability

The manuscript contains the majority of the data generated in the current work. Any additional information that may be required can be requested from the corresponding author on a reasonable basis.

Acknowledgements

The authors extend their appreciation to the Deanship of Research and Graduate Studies at King Khalid University, Saudi Arabia, through Large Research Project under grant number RGP-2/685/46. The work is also supported by Open Foundation of Hainan International Joint Research Center of Marine Advanced Photoelectric Functional Materials (2024MAPFM01).

References

1 U. Nishan, S. U. Haq, A. Rahim, M. Asad, A. Badshah, A.-u.-H. Ali Shah, *et al.*, Ionic-liquid-stabilized TiO_2 nanostructures: a platform for detection of hydrogen peroxide, *ACS Omega*, 2021, **6**, 32754–32762.
2 K. Nakashima, M. Wada, N. Kuroda, S. Akiyama and K. Imai, High-performance liquid chromatographic determination of hydrogen peroxide with peroxyoxalate chemiluminescence detection, *J. Liq. Chromatogr. Relat. Technol.*, 1994, **17**, 2111–2126.
3 F. Zhao, S. Zhou and Y. Zhang, Ultrasensitive detection of hydrogen peroxide using Bi2Te3 electrochemical sensors, *ACS Appl. Mater. Interfaces*, 2021, **13**, 4761–4767.
4 Y.-C. Shiang, C.-C. Huang and H.-T. Chang, Gold nanodot-based luminescent sensor for the detection of hydrogen peroxide and glucose, *Chem. Commun.*, 2009, 3437–3439.
5 A. Pashkova, K. Svajda, G. Black and R. Dittmeyer, Automated system for spectrophotometric detection of liquid phase hydrogen peroxide for concentrations up to 5% w/w, *Rev. Sci. Instrum.*, 2009, **80**(5), 055104.

6 Z. Mao, Z. Qing, T. Qing, F. Xu, L. Wen, X. He, *et al.*, Poly (thymine)-templated copper nanoparticles as a fluorescent indicator for hydrogen peroxide and oxidase-based biosensing, *Anal. Chem.*, 2015, **87**, 7454–7460.

7 U. Nishan, A. Ahmed, N. Muhammad, M. Shah, M. Asad, N. Khan, *et al.*, Uric acid quantification via colorimetric detection utilizing silver oxide-modified activated carbon nanoparticles functionalized with ionic liquid, *RSC Adv.*, 2024, **14**, 7022–7030.

8 M. Asad, N. Muhammad, N. Khan, M. Shah, M. Khan, M. Khan, *et al.*, Colorimetric acetone sensor based on ionic liquid functionalized drug-mediated silver nanostructures, *J. Pharm. Biomed. Anal.*, 2022, **221**, 115043.

9 Y. Chen, Q. Zhong, Y. Wang, C. Yuan, X. Qin and Y. Xu, Colorimetric detection of hydrogen peroxide and glucose by exploiting the peroxidase-like activity of papain, *RSC Adv.*, 2019, **9**, 16566–16570.

10 X. Cheng, L. Huang, X. Yang, A. A. Elzatahry, A. Alghamdi and Y. Deng, Rational design of a stable peroxidase mimic for colorimetric detection of H_2O_2 and glucose: A synergistic CeO_2/Zeolite Y nanocomposite, *J. Colloid Interface Sci.*, 2019, **535**, 425–435.

11 L. Challier, F. Gal, G. Carrot, H. Perez and V. Noel, Hybrid platinum nanoparticle ensemble for the electrocatalytic oxidation of H_2O_2: Toward nanostructured biosensor design, *Electrochem. Commun.*, 2013, **28**, 118–121.

12 M. Nasir, S. Rauf, N. Muhammad, M. H. Nawaz, A. A. Chaudhry, M. H. Malik, *et al.*, Biomimetic nitrogen doped titania nanoparticles as a colorimetric platform for hydrogen peroxide detection, *J. Colloid Interface Sci.*, 2017, **505**, 1147–1157.

13 L. Sun, Y. Ding, Y. Jiang and Q. Liu, Montmorillonite-loaded ceria nanocomposites with superior peroxidase-like activity for rapid colorimetric detection of H_2O_2, *Sens. Actuators, B*, 2017, **239**, 848–856.

14 Y.-Y. Tsai, J. Oca-Cossio, K. Agering, N. E. Simpson, M. A. Atkinson, C. H. Wasserfall, *et al.*, Novel synthesis of cerium oxide nanoparticles for free radical scavenging, *Nanomedicine*, 2007, **2**, 325–332.

15 J. Gao, Z. Si, Y. Xu, L. Liu, Y. Zhang, X. Wu, *et al.*, Pd–Ag@ CeO_2 catalyst of core–shell structure for low temperature oxidation of toluene under visible light irradiation, *J. Phys. Chem. C*, 2018, **123**, 1761–1769.

16 N. Mojoudi, N. Mirghaffari, M. Soleimani, H. Shariatmadari, C. Belver and J. Bedia, Phenol adsorption on high microporous activated carbons prepared from oily sludge: equilibrium, kinetic and thermodynamic studies, *Sci. Rep.*, 2019, **9**, 19352.

17 G. Jayakumar, A. A. Irudayaraj and A. D. Raj, Investigation on the synthesis and photocatalytic activity of activated carbon–cerium oxide (AC–CeO_2) nanocomposite, *Appl. Phys. A*, 2019, **125**, 742.

18 G. Murugadoss, D. D. Kumar, M. R. Kumar, N. Venkatesh and P. Sakthivel, Silver decorated CeO2 nanoparticles for rapid photocatalytic degradation of textile rose bengal dye, *Sci. Rep.*, 2021, **11**, 1080.

19 Y. Li, S. Li, R. Zhou, G. Li and X. Li, Selective laser welding in liquid: A strategy for preparation of high-antibacterial activity nanozyme against Staphylococcus aureus, *J. Adv. Res.*, 2023, **44**, 81–90.

20 K. Wu, L. Zhou, C.-J. Jia, L.-D. Sun and C.-H. Yan, Pt-embedded-CeO 2 hollow spheres for enhancing CO oxidation performance, *Mater. Chem. Front.*, 2017, **1**, 1754–1763.

21 U. Nishan, I. Ullah, N. Muhammad, S. Afridi, M. Asad, S. U. Haq, *et al.*, Investigation of silver-doped iron oxide nanostructures functionalized with ionic liquid for colorimetric sensing of hydrogen peroxide, *Arabian J. Sci. Eng.*, 2023, **48**, 7703–7712.

22 X. Huang, H. Zhou, Y. Huang, H. Jiang, N. Yang, S. A. Shahzad, *et al.*, Silver nanoparticles decorated and tetraphenylethene probe doped silica nanoparticles: a colorimetric and fluorometric sensor for sensitive and selective detection and intracellular imaging of hydrogen peroxide, *Biosens. Bioelectron.*, 2018, **121**, 236–242.

23 H. Liu, L. Zhu, H. Ma, J. Wen, H. Xu, Y. Qiu, *et al.*, Copper (II)-coated Fe_3O_4 nanoparticles as an efficient enzyme mimic for colorimetric detection of hydrogen peroxide, *Microchim. Acta*, 2019, **186**, 1–9.

24 W. Yang, C. Weng, X. Li, H. He, J. Fei, W. Xu, *et al.*, A sensitive colorimetric sensor based on one-pot preparation of h-Fe_3O_4@ppy with high peroxidase-like activity for determination of glutathione and H2O2, *Sens. Actuators, B*, 2021, **338**, 129844.

25 J. Lian, D. Yin, S. Zhao, X. Zhu, Q. Liu, X. Zhang, *et al.*, Core-shell structured Ag-CoO nanoparticles with superior peroxidase-like activity for colorimetric sensing hydrogen peroxide and o-phenylenediamine, *Colloids Surf., A*, 2020, **603**, 125283.

26 H. Chen, Q. Shi, G. Deng, X. Chen, Y. Yang, W. Lan, *et al.*, Rapid and highly sensitive colorimetric biosensor for the detection of glucose and hydrogen peroxide based on nanoporphyrin combined with bromine as a peroxidase-like catalyst, *Sens. Actuators, B*, 2021, **343**, 130104.

27 A. Chakraborty and H. Acharya, Magnetically separable Fe3O4 NPs/MIL-53 (Al) nanocomposite catalyst for intrinsic OPD oxidation and colorimetric hydrogen peroxide detection, *Colloids Surf., A*, 2021, **624**, 126830.

28 K. Aneesh and S. Berchmans, Enhanced peroxidase-like activity of CuWO4 nanoparticles for the detection of NADH and hydrogen peroxide, *Sens. Actuators, B*, 2017, **253**, 723–730.

29 F. Zarif, S. Rauf, S. Khurshid, N. Muhammad, A. Hayat, A. Rahim, *et al.*, Effect of pyridinium based ionic liquid on the sensing property of Ni0 nanoparticle for the

colorimetric detection of hydrogen peroxide, *J. Mol. Struct.*, 2020, **1219**, 128620.

30 U. Nishan, T. Zahra, A. Badshah, N. Muhammad, S. Afridi, M. Shah, *et al.*, Colorimetric sensing of hydrogen peroxide using capped Morus nigra-sawdust deposited zinc oxide nanoparticles via Trigonella foenum extract, *Front. Bioeng. Biotechnol.*, 2024, **12**, 1338920.